

High-purity and stable single-photon emission in bilayer WSe₂ via phonon-assisted excitation

Claudia Piccinini,¹ Athanasios Paralikis,¹ José Ferreira Neto,¹ Abdulmalik A. Madigawa,¹ Pawel Wyborski,¹ Vikas Remesh,² Luca Vannucci,¹ Niels Gregersen,¹ and Battulga Munkhbat^{1,*}

¹*Department of Electrical and Photonics Engineering, Technical University of Denmark, 2800, Kgs. Lyngby, Denmark*

²*Institut für Experimentalphysik, Universität Innsbruck, 6020 Innsbruck, Austria*

The excitation scheme is essential for single-photon sources as it prepares the exciton state, defines the decay dynamics, and influences the spectral diffusion of the emitted single photons. Here, we investigate the impact of different optical excitation strategies on the single-photon emission characteristics of bilayer WSe₂ quantum emitters. Under phonon-assisted excitation, we achieve narrow and stable single-photon emission with an excellent purity reaching 0.94 ± 0.02 . Furthermore, the decay time is reduced by more than an order of magnitude from (16.65 ± 2.39) ns for above-band excitation to (1.33 ± 0.04) ns for phonon-assisted excitation. Finally, we observe a suppressed spectral wandering along with a two-fold reduction of the spectral linewidth. Our comprehensive investigation highlights the critical role of the excitation method in optimizing the performance of WSe₂-based quantum emitters.

I. INTRODUCTION

A key component in optical quantum information technologies is an on-demand source of single photons, which serves as the source of quantum bits that encode information [1]. The fundamental requirement for a usable source is single photon emission with near-unity purity, efficiency, and indistinguishability. Spontaneous parametric down-conversion [2] in a nonlinear material is a well-established method to generate highly indistinguishable photons [3]. However, its probabilistic nature limits the efficiency to merely a few percent. On the other hand, a two-level system [4] allows for the deterministic emission of single photons through the spontaneous emission process. Recently, highly efficient emission of indistinguishable photons has been achieved from semiconductor quantum dots [5–7] placed in carefully engineered microstructures. Nevertheless, epitaxial growth of high-quality quantum dot material requires advanced and costly epitaxy tools. As an alternative, quantum emitters in two-dimensional (2D) transition metal dichalcogenides (TMDs) materials have recently emerged as an attractive platform for deterministic single-photon emission [8–13]. Such a platform provides several advantages, including accessible cost-effective materials, deterministic fabrication methods [14–16], and ease of integration with photonic [17] and plasmonic systems [18, 19]. Additionally, the reduced dimensionality of TMDs facilitates efficient light extraction [20]. Consequently, single-photon emission over a broad spectrum from visible [21] to telecom ranges [22] has been demonstrated from mono- and few-layer TMDs via strain- and defect engineering [15, 23–26].

Despite significant efforts in developing high-quality quantum emitters in TMDs, the efficient generation of indistinguishable single photons from these platforms remains an open fundamental challenge. Spectral diffusion

and phonon-induced dephasing are the primary obstacles that can be addressed through various strategies. These include integrating a high-Q resonant cavity [27], introducing electrical contacts to stabilize the charge environment, and implementing advanced optical excitation schemes. Recently, a strategy of coupling these quantum emitters to a resonant open cavity has been successfully demonstrated, exhibiting state-of-the-art efficiency as high as 65% to the first-lens but limited indistinguishability of around 2% [27]. This strategy was later employed to engineer the coherence of the emitted photons by selectively boosting the emission of the zero-phonon line [28]. Additionally, the spectral diffusion of the emitted photons has been improved via hBN encapsulation [15, 29] as well as with electrical contacts [30].

At the same time, the pumping scheme also has a significant impact on the figures of merit of generated single photons from any two-level quantum emitter platform [31]. Above-band optical excitation has limitations on photon indistinguishability [32] due to the presence of photo-induced charges. In contrast, resonant excitation of quantum emitters has resulted in near-unity indistinguishability [33] but at the cost of a maximum 50% collection efficiency in the cross-polarization setup. Alternatively, phonon-assisted excitation represents an attractive trade-off combining efficient population inversion and good photon indistinguishability [34, 35]. Recently, efficient population inversion in TMD quantum emitters with high preparation fidelity above 99% has been theoretically predicted under phonon-assisted excitation [35]. However, to date, proper implementation of phonon-assisted excitation and its systematic comparison with other excitation schemes have not been experimentally demonstrated in TMD quantum emitters.

In this work, we implement three optical excitation schemes, i.e., above-band, near-resonant, and phonon-assisted, and systematically investigate their impacts on basic single-photon properties of bilayer WSe₂ quantum emitters. First, we demonstrate high single-photon

* bamunk@dtu.dk

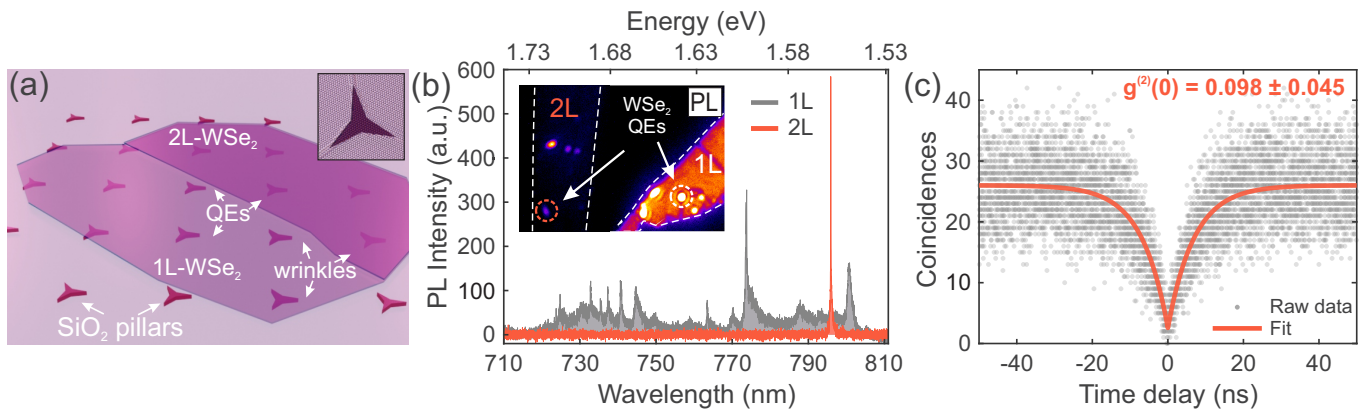


FIG. 1. **Quantum emitters in mono- and bilayer WSe₂**. (a) Sketch of mono- (1L) and bilayer (2L) flake deposited on top of star-shaped nanostructures leading to the formation of nanowrinkles in correspondence of their vertex. The nanowrinkles host the quantum emitters. (b) μ PL spectra of the two bright spots in 1L WSe₂ (grey) and 2L WSe₂ (red) encircled in the inset image, integrated over 1 s. They show typical emission imprints of the two different thicknesses' flakes. A 700 nm long-pass filter was applied to prevent the coupling of the reflected laser. Inset: color-coded PL image of the sample taken at $T = 4$ K. The white dashed lines highlight the contours of the 1L and 2L flakes. (c) Second-order correlation measurement of emitter Q1 from the bilayer spot (red dashed circle in inset in (b)) under CW LED excitation at 470 nm. The fit reveals a $g^{(2)}(0)$ value of 0.098 ± 0.045 .

purity, reaching 0.921 ± 0.015 and 0.943 ± 0.018 under pulsed above-band and near-resonant excitations, respectively. Near-resonant yields shorter and simpler decay dynamics, with a decay constant of 12.62 ± 1.18 ns. More importantly, under the phonon-assisted excitation, we achieved much faster decay rates ($\tau = 1.33 \pm 0.04$ ns) and a two-fold reduction in spectral diffusion of the emission line from bilayer WSe₂ quantum emitters, in contrast to above-band excitation. Our work contributes to the fundamental understanding of WSe₂ quantum emitter platform and to its application in future quantum photonics.

II. SYSTEM UNDER STUDY: MONO- AND BILAYER WSe₂ QUANTUM EMITTERS

We begin our study by preparing highly-polarized single-photon emitters out of WSe₂ flakes through deterministic strain engineering as illustrated in Fig.1(a). Mechanically exfoliated mono- and bilayer WSe₂ flakes were transferred onto a thermally oxidized silicon substrate ($d_{\text{SiO}_2} = 110$ nm) featuring an array of star-shaped nanostructures (see Methods for the details). The nanostructures form one-dimensional nanowrinkles that host linearly-polarized quantum emitter [36]. To investigate the optical properties of the fabricated samples, we mounted the sample in an optical cryostat operating at 4 K. The cryostat is equipped with nanopositioners and a low-temperature objective lens (NA = 0.82, 60 \times). Initially, a low-temperature photoluminescence (PL) image of the sample was acquired under 470 nm LED excitation. A 700 nm long-pass optical filter was employed to eliminate reflected signals from the excitation. As depicted in the inset of Fig. 1(b), the PL image reveals bright spots originating from the strain-induced mono- and bi-

layer WSe₂, which are distinctly contrasted against the emission signal from the planar, unstrained flakes.

For a quantitative comparison between the mono and bi-layer emitters, we measured the PL spectra of the individual bright spot regions of each under a 532 nm pulsed excitation (pulse duration 200 ps, repetition rate 80 MHz) using a spectrometer ($f = 550$ mm, 1200 grooves/mm grating). Fig. 1(b) shows the emission spectra obtained from two exemplary mono- and bilayer regions (dashed red and white circles in the inset) hosting strain-engineered quantum emitters. The monolayer emission spectrum exhibits numerous intense and narrow emission lines spreading across a broad spectral range of 720 - 810 nm on top of a broad, weak emission background from the planar monolayer. The observed narrow lines are attributed to single-photon emission from several different emitters [8, 9, 12], while the broad background is ascribed to the emission from the planar monolayer region around the emitter due to the diffraction-limited collection spot. On the other hand, the bilayer quantum emitter presents a single isolated narrow emission line (FWHM = 0.14 nm) without any noticeable background. Moreover, the distribution of the narrow peaks in the bilayer spans within the range of 790 - 810 nm. Surprisingly, despite the bilayer WSe₂ host being an indirect bandgap, the intensities of the emission lines are comparable to those observed in the monolayer under identical experimental conditions (more exemplary spectra in Fig. S1 in the Supporting Information).

Considering the previous observations, we focus on the WSe₂ bilayer quantum emitters since their characteristics make them preferable for our study. We obtained the single-photon purity of the bilayer quantum emitters by measuring the second-order correlation of a representative emission line under continuous-wave (CW) exci-

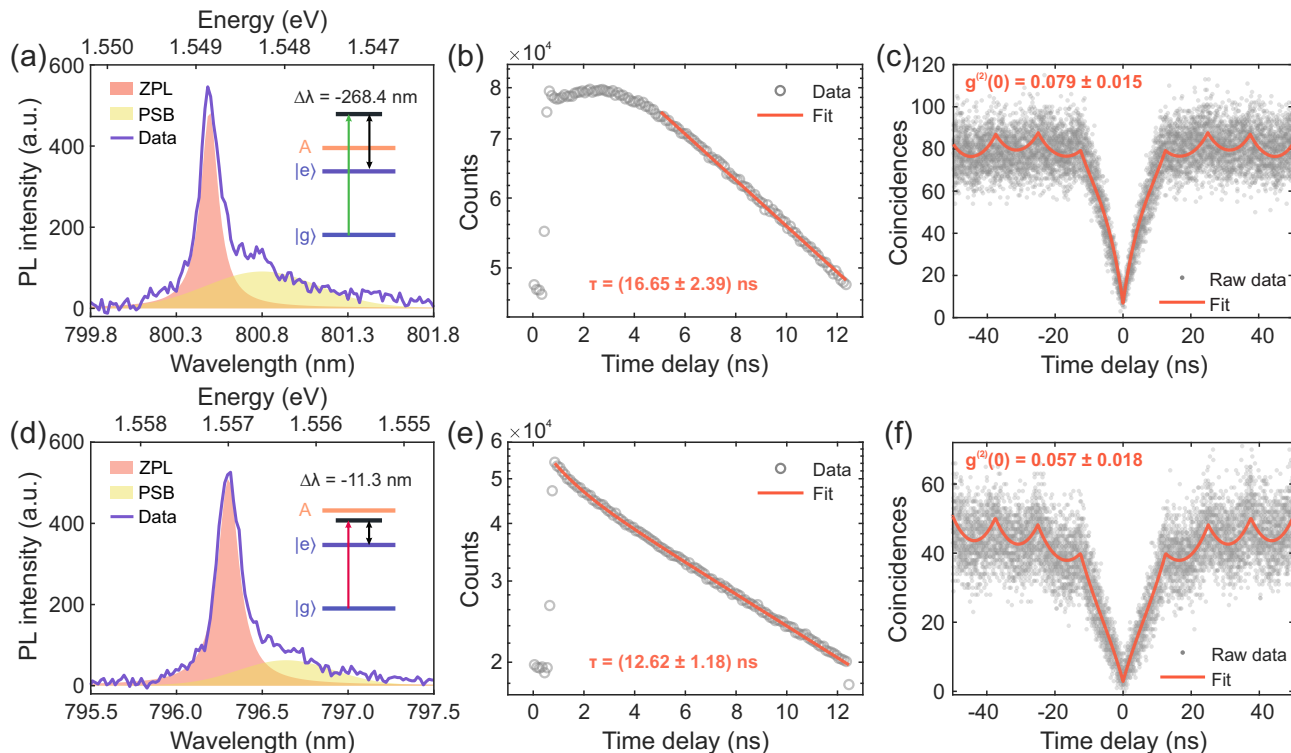


FIG. 2. **Above-band and near-resonant excitations.** Emission spectra of emitter Q1 under pulsed above-band excitation at 532 nm (a) and emitter Q2 under near-resonant pulsed excitation at 785 nm (d). The graphs present fittings to the raw data (solid purple line) with a sum of a Lorentzian (red area) and a Gaussian (yellow area) accounting for the contribution from the ZPL and the PSB, respectively. The inset schemes on the right show a simplified band diagram of the emitters as a two-level system with the respective pumping energy. (b) Semi-logarithmic plot of the time-resolved PL measurement from Q1 (grey circles) with relative single decay exponential fitting function (red line) with a constant $\tau_1 = (16.65 \pm 2.39)$ ns. (c) Second-order intensity correlation measurement ($g^{(2)}(\tau)$) of (a) (Q1) under the same pulsed excitation. From the double exponential fit (red line), we extract an antibunching value of $g^{(2)}(0) = 0.079 \pm 0.015$. (e) Semi-logarithmic plot of the time-resolved PL measurement from Q2 (grey circles) with relative double decay exponential fitting function (red line). The two extracted time constants are $\tau_1 = (12.62 \pm 1.18)$ ns and $\tau_2 = (1.14 \pm 0.21)$ ns, accounting for 96.5% and 3.5% of the fit curve, respectively. (f) Second-order intensity correlation measurement of (d) under the same pulsed excitation as in (d) and (e). The $g^{(2)}(0)$ value extracted is 0.057 ± 0.018 . The measurements in (b) and (e) are integrated over 3 minutes, while those in (c) and (f) over 8 hours.

tation at 470 nm. A 750 nm long-pass filter helps suppress the emitted light from the laser light. The measurement is performed with a Hanbury Brown-Twiss (HBT) setup, which includes a 50:50 fiber beam splitter and a pair of superconducting nanowire single-photon detectors (SNSPDs). In Fig. 1(c), we show the obtained correlation histogram as a function of delay, which exhibits a strong antibunching behavior. The suppressed coincidence counts at zero time delay establish the clear single-photon nature of the emission with extracted single-photon purity of $g^{(2)}(0) = 0.098 \pm 0.045$.

III. ABOVE-BAND VS. NEAR-RESONANT OPTICAL EXCITATION

To systematically compare the effect of the above-band and the near-resonant excitation schemes on the bilayer quantum emitters, we conducted an investigation of the

optical properties of two emitters (Q1 and Q2). Our study includes high-resolution emission spectra, lifetime, and purity. We analyze the differences to find the most effective approach for optimal performance.

Above-band optical excitation. Here, we use the 532 nm pulsed laser excitation. Fig. 2(a) shows the obtained μ PL spectrum from Q1, revealing a narrow zero-phonon line (ZPL) at 800.5 nm and a visible broad phonon side-band (PSB). By fitting a Lorentzian and a Gaussian function to the ZPL and to the PSB, respectively, we qualitatively extract a width of 0.124 nm (0.242 meV) for the ZPL and 0.782 nm (1.513 μ eV) for the PSB, and a Debye-Waller factor $I_{\text{ZPL}}/(I_{\text{ZPL}} + I_{\text{PSB}})$ of 0.551 (Fig. 2(a)). This suggests a strong exciton-phonon coupling, which is in good agreement with previous reports [35, 37, 38]. Notably, the ZPL is orders of magnitude broader than its Fourier-limited value of 57.0×10^{-6} nm (0.11 μ eV), considering the decay time of 16.65 ns (see next paragraph). This suggests that

the pure dephasing contribution to the homogeneous linewidth is substantial, consequently resulting in lower indistinguishability [30].

For the characterization of the dynamic behavior of individual quantum emitter under above-band excitation, we carried out a time-resolved PL (TRPL) measurement. As shown in 2(b), we observe a relatively fast decay at shorter time delays (≤ 0.5 ns), after which the curve rises again and reaches its maximum at around 3 ns. We attribute this to trapped states involved in the population of the excited state [39, 40]. At longer delay times, the decay is fitted with a single exponential (red line), revealing a decay time of $\tau = (16.65 \pm 2.39)$ ns (st. error). Such value is in good agreement with previous observations on TMD single-photon sources [36, 41, 42]. The second-order correlation measurement under pulsed above-band excitation, shown in Fig. 2(c), reveals a $g^{(2)}(0)$ of 0.079 ± 0.015 . The extracted value is consistent with the one in Fig. 1(c) under CW operation, indicating a good single-photon purity also under triggered excitation.

Near-resonant optical excitation. To perform the near-resonant excitation, we scanned the pulsed laser from 730 nm up to 790 nm, corresponding to detuning $\Delta\lambda = \lambda_{\text{laser}} - \lambda_X$ from -66.3 nm to -6.3 nm with respect to the quantum emitter ($\lambda_X = 796.3$ nm), in steps of 10 nm. Since the energy corresponding to this pumping wavelength is below the energy of the A-exciton of planar WSe₂ [43], but above the excitonic transition energy considered (c.f. the band diagram scheme in the inset of Fig. 2(d)), we refer to such a detuning as *near-resonant*. We observed that the quantum emitter could be excited over a large range of detuning (see Supporting Information Note 2 for details). This behavior has been previously reported in WSe₂ [9, 44] based on photoluminescence excitation spectroscopy measurement. In our case, the maximum emission intensity occurred when the laser is detuned to $\Delta\lambda = -11.3$ nm (9.1 meV) from the emission line, with results reported in Figs. 2(d)-(e). At this detuning, the zero-phonon line and phonon sideband linewidth of the emitter (Q2) are found to be 0.124 nm and 0.760 nm respectively. From this, we compute the Debye-Waller factor as $DWF = 0.538$. (Fig. 2(d)). Additionally, under near-resonant excitation, we achieved a $g^{(2)}(0)$ value of 0.057 ± 0.018 . These results are similar to those obtained under the above-band excitation (Fig. 2(f)) and suggest that the emission spectrum and single-photon purity of this particular quantum emitters may not be heavily dependent on the excitation scheme.

However, a striking dissimilarity between the two excitation schemes arises from the time-resolved measurement. As shown in Fig. 2(e), the obtained lifetime histogram under near-resonant excitation exhibits much simpler behavior compared, revealing a predominant single exponential decay contribution with a time constant of $\tau = (12.62 \pm 1.18)$ ns. This particular contrast in decay dynamics under the near-resonant excitation can be attributed to the quantum emitter being optically excited

near its bandgap. These experimental results suggest that directly populating a bilayer quantum emitter with a proper excitation scheme is essential to avoid unnecessary internal relaxation processes and the creation of additional unwanted photo-induced charge carriers, resulting in simpler dynamics and reduced lifetime.

IV. THEORY: POPULATION INVERSION UNDER LA-PHONON-ASSISTED EXCITATION

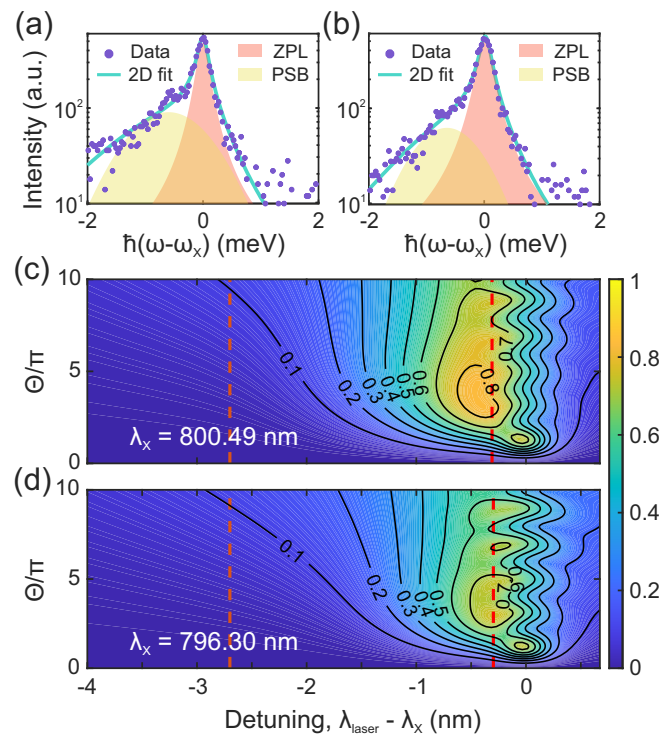


FIG. 3. Theory of exciton-phonon coupling and pulsed excitation. (a, b): Experimental data and fitted theoretical curves for the PL spectrum in the presence of phonon coupling for emitter Q1 (a) and Q2 (b). Separate contributions to ZPL and PSB are highlighted for visual clarity using Lorentzian and Gaussian fits, respectively. (c, d) Population inversion as a function of the wavelength detuning $\lambda_{\text{laser}} - \lambda_X$ and the pulse amplitude Θ calculated theoretically for emitters Q1 (c) and Q2 (d). The laser pulse has a FWHM of 0.30 nm ($t_p = 2.65$ ns in our notation). Dashed orange and red lines are placed at detunings of -2.7 nm and -0.3 nm, respectively.

The rather low Debye-Waller factor previously obtained from the exemplary PL spectra under above-band and near-resonant excitation suggests a strong exciton-phonon interaction. A quantitative analysis of phonon coupling is performed by fitting the PL spectra in Figs. 2(a) and 2(d) to the theoretical prediction obtained from an independent boson model, including the coupling to 2D acoustic phonons. Such a fit enables the reconstruction of the 2D phonon spectral density $J(\omega) = \alpha\omega^2 \exp(-\omega^2/\omega_c^2)$ under above-band and near-resonant

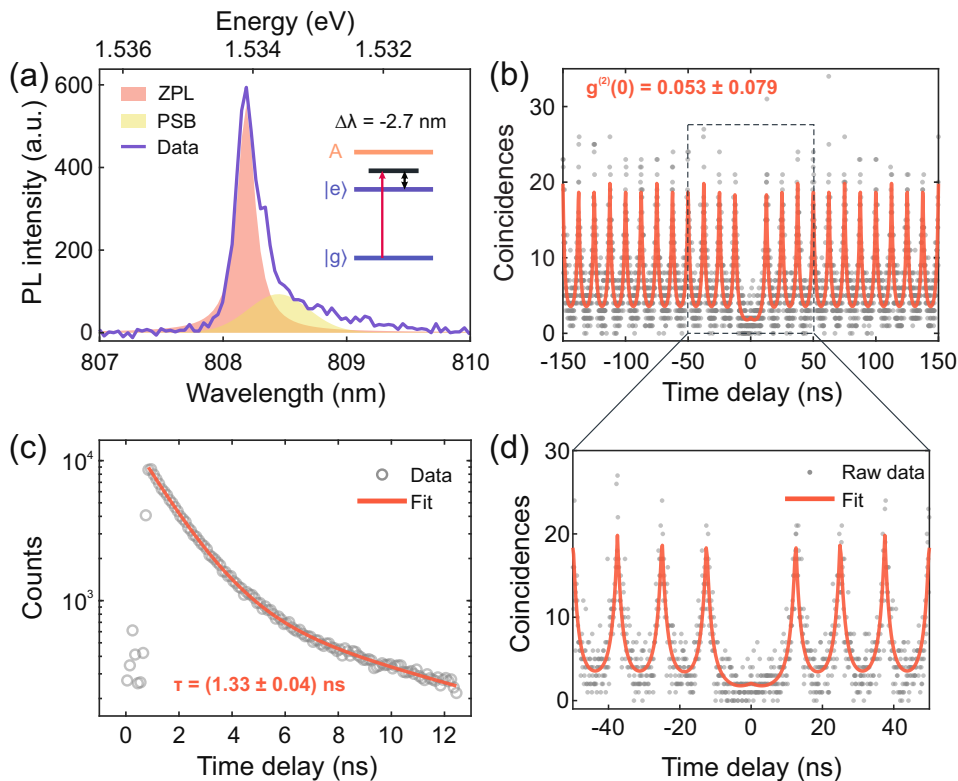


FIG. 4. **Phonon-assisted excitation.** (a) PL spectrum of emitter Q3 under pulsed excitation at detuning of -2.7 nm from the quantum emitter. The fit function on the raw data (purple) is a sum of a Lorentzian (red area) and a Gaussian (yellow area) accounting for the contribution from the ZPL and the PSB, respectively. The inset shows a simplified band diagram of an emitter as a two-level system highlighting the pumping energy detuning. (b) Second-order autocorrelation measurement of Q3. From the double exponential fit (red line), we extract an antibunching value of $g^{(2)}(0) = 0.053 \pm 0.079$. (c) Time-resolved PL measurement from Q3 in a semilogarithmic plot with relative double exponential fitting function with extracted time constants of $\tau_1 = (1.33 \pm 0.04)$ ns (80.4%) and $\tau_2 = (8.31 \pm 6.29)$ ns (19.6%). (d) Replot of $g^{(2)}(\tau)$ in (c) for time delays up to ± 50 ns.

excitation conditions, respectively (see Methods section for detailed information). As shown in Figs. 3(a) and 3(b), we find good agreement between theory and experiments, with the extracted fit parameters reported in the SI. We calculate a Huang-Rhys factor $S = \frac{\sqrt{\pi}}{2} \omega_c \alpha$ of 0.53 and 0.38 for emitters Q1 and Q2, respectively, indicating indeed a strong coupling to the phonon environment.

Next, we calculate the predicted population inversion under pulsed laser excitation for emitters Q1 and Q2 and for wavelength detuning up to $\Delta\lambda = -4$ nm. The excited state population after a Gaussian electric field pulse $\Omega(t) = \frac{\Theta}{\sqrt{\pi}t_p} e^{-(t/t_p)^2}$, with $\Theta = \int_{-\infty}^{+\infty} dt \Omega(t)$ the pulse area, is shown in Figs. 3(c) and 3(d), where we also include a suitable spectral broadening as obtained from the fit (see Methods section). Both emitters yield overall very similar results, with a sizable population > 0.7 obtained at a detuning $\Delta\lambda \approx -0.5$ nm and for a moderate pulse area of $3-5\pi$. We interpret these results as a signature of LA phonon-assisted excitation, where a laser pulse with a shorter wavelength than the exciton is able to populate the excited state by exciting additional phonon modes. The optimal detuning corresponds indeed to the maximum of the phonon spectral density. While the signal

decreases monotonically for larger detuning, we still observe population > 0.1 at $\Delta\lambda = -3$ nm for a larger pulse area of 10π , due to the strong phonon coupling in these quantum emitters. Close to resonance ($\Delta\lambda \approx 0$), we also observe the signature of Rabi oscillations as a function of the pulse area. Our results highlight the relevance of phonon dressing for optical excitation of WSe₂ quantum emitters in the near-resonant regime.

V. LA-PHONON-ASSISTED EXCITATION

Single-photon characterization. To experimentally demonstrate acoustic phonon-assisted excitation on WSe₂ bilayer quantum emitters, we tune the pump laser wavelength from $\Delta\lambda = -3.0$ nm to $\Delta\lambda = -0.1$ nm with respect to the zero-phonon line. First, we notice that some emission from Q1 and Q2 is observed already at $\Delta\lambda = -3.0$ nm, consistently with the theoretical predictions in Figs. 3(c) and (d). Then, we consider another bilayer quantum emitter (Q3), and we tune the excitation laser to $\Delta\lambda = -2.7$ nm (5 meV) to ensure uncomplicated spectral filtering of the laser light from the single-

photon emission while maintaining a sufficient population inversion probability. Fig. 4(a) shows the obtained PL spectrum, revealing an emission line at 808.2 nm. The extracted FWHM with a Lorentzian fit of the ZPL is 0.174 nm (0.33 meV), approximately 40% larger compared to Q1 and Q2 under above-band and near-resonant excitation. Note that the Debye-Waller factor under this excitation has increased up to 0.712. The broader ZPL compared to those in Figs. 2(a) and (d) can be attributed to the fact that pulsed excitation at detuning of -2.7 nm (5 meV) requires high excitation power, potentially resulting in additional line broadening (see Supporting Information 3 for the power-dependent PL spectra).

The second-order correlation measurement (see Fig. 4(b)) shows a $g^{(2)}(0)$ of 0.053 ± 0.079 , establishing highly pure single-photon emission similar to that under above-band (Fig. 2(c)) and near-resonant (Fig. 2(f)) excitation. However, the most remarkable observation is the shortened decay time of bilayer quantum emitter emission under phonon-assisted excitation. The double exponential fit on the time-resolved PL data presented in Fig. 4(c) suggests that 80.4% of the contribution to the emitted light has a decay time of (1.33 ± 0.04) ns. This is among the shortest reported in the literature of WSe₂-based quantum emitters on a dielectric substrate without any cavity. The relevance of this result lies in the fact that faster exciton recombination paves the way for a deterministically triggered source at a higher rate for future quantum computing devices based on WSe₂ quantum emitters. Besides that, the additional low contribution (below 20% of the total integrated counts) of longer decay time $\tau = (8.31 \pm 6.29)$ ns can be attributed to some additional slow carrier recombination processes within the bilayer quantum emitter.

Notably, pumping at $\Delta\lambda = -2.7$ nm could also be explained with different mechanisms than LA phonon-assisted, such as excitation through higher-order dark states [45] and charged states [46]. This is, however, not contemplated by the theoretical two-level model presented above. Advanced modeling and thorough experimental investigation are needed to assess the contribution of these additional states in the exciton population process. On the other hand, coupling to optical phonons can be safely ruled out, as their absorption energy is predicted to occur at a larger spectral detuning of approximately $\Delta\lambda = -10.4$ nm or more [47–50]

Spectral diffusion. An unambiguous signature of phonon-assisted excitation is obtained at shorter detuning $\Delta\lambda = -0.3$ nm, where our theory predicts population inversion above 80% for proper pulse amplitude. In the following, we evaluate and compare the line broadening and the spectral diffusion under phonon-assisted and above-band excitations. The former is an indicator of energy shift of the quantum emitter energy in time scales faster than the experimental acquisition time, while the latter can be traced over the measurement time scale.

In Figs. 5(a) and (b) (same scale), we report the PL spectra under the two excitation schemes at $\Delta\lambda =$

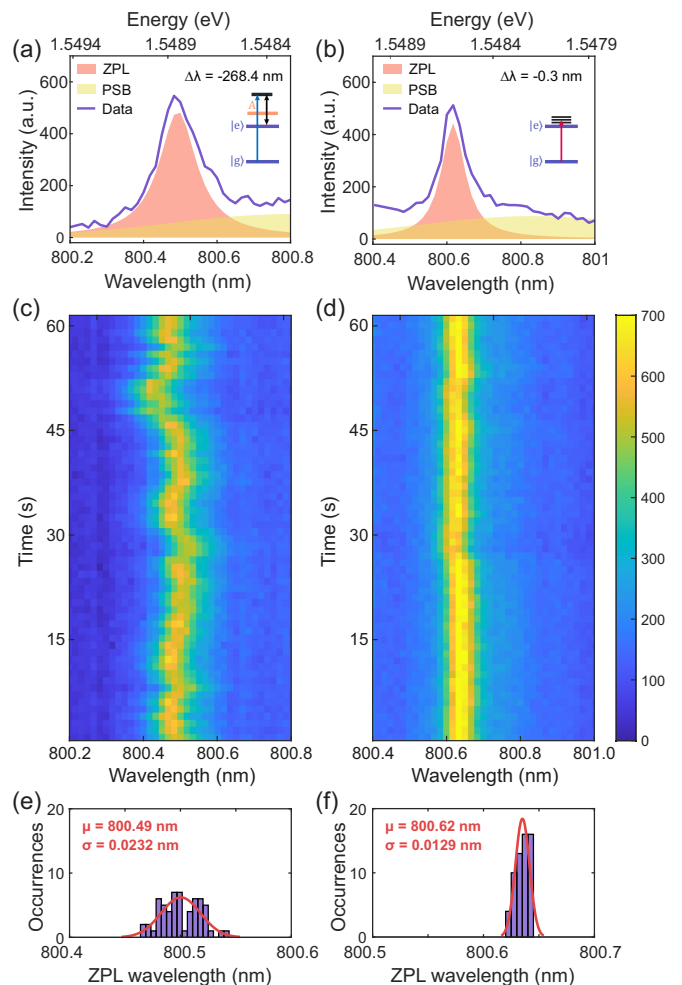


FIG. 5. Spectral diffusion under phonon-assisted excitation. High-resolution PL spectra at time 1 s (a, b) and their time evolution (c, d) for above-band excitation and phonon-assisted excitation, respectively. The maps consist of one horizontal line every second, with 0.7 s integration time for each one of them. The complementary 0.3 s is the time required to open and close the spectrometer’s shutter. (e) and (f) show the statistical analysis of the central wavelength of the ZPL as extracted from the fitting of each line in the map. The red curves are Gaussian fittings of the obtained distributions. The mean value and the standard deviation in (e) are $\mu_{\text{ZPL}} = 800.49$ nm and $\sigma_{\text{ZPL}} = 0.0232$ nm, respectively. At the same time, their values for (f) are $\mu_{\text{ZPL}} = 800.62$ nm and $\sigma_{\text{ZPL}} = 0.0129$ nm.

-268.4 nm (above-band) and $\Delta\lambda = -0.3$ nm (acoustic phonon-assisted) for the same emitter. The spectra exhibit a significant difference in terms of the emission linewidth. In the case of the phonon-assisted excitation, the extracted FWHM from the Lorentzian fitting results is 0.074 nm (151 μeV). This value is close to the nominal resolution of our spectrometer (0.05 nm), which might, thus, not allow us to resolve the true linewidth of the emission and give a counterfeit value. Anyhow, the obtained value is 1.5 times narrower than the FWHM of

0.108 nm from the spectrum under the below-saturation above-band excitation. This might suggest that a more stable charge environment is achieved under the phonon-assisted excitation without the creation of additional photo-induced charges, resulting in lower spectral diffusion. To visualize the spectral diffusion of the emission line, we recorded the emission signal as a function of time under both excitation schemes. Remarkably, the spectral diffusion at a time scale slower than the experimental acquisition time is drastically reduced as well, as clearly visible from the time evolution of the μ PL spectrum in Figs. 5(c) and 5(d). In both maps, each horizontal line corresponds to 1 second of measurement, during which the PL emission is integrated over 0.7 sec. By fitting each spectrum with a Lorentzian function, we can extract the resonance of the ZPL as a function of time. The histogram plots in Figs. 5(e) and (f) show the number of occurrences in the wavelength range of emission, grouped up in 0.005 nm-broad bins. Fitting the histograms with a Gaussian function allows us to extract a mean value of $\mu_{\text{ZPL}} = 800.49$ nm and a standard deviation of $\sigma_{\text{ZPL}} = 0.0232$ nm for the distribution of the peaks' central position under above-band excitation and $\mu_{\text{ZPL}} = 800.62$ nm and $\sigma_{\text{ZPL}} = 0.0129$ nm under acoustic phonon-assisted excitation, thereby proving that the latter reduces both the inhomogeneous broadening of the ZPL and its spectral diffusion as compared to above-band excitation. Both these effects are critical obstacles to single-photon indistinguishability, which requires a transform-limited linewidth, identical emission energy, and well-defined polarization.

The results presented in the previous sections demonstrate that the exciton preparation scheme affects the characteristics of the emitted single photons substantially. Employing a proper pumping strategy is necessary to achieve high purity, fast dynamics, and minimal spectral diffusion. All the excitation schemes presented in this work rely on incoherent processes. In particular, the phonon-assisted scheme provides both efficient population inversion and improved spectral stability, which are inescapable premises for a future efficient and indistinguishable source of single photons from bilayer WSe₂. However, coherent state preparation is essential to increase the coherence time and to generate superposition states, which are at the base of quantum computing and quantum information processing. In this regard, the strictly resonant (in a cross-polarization configuration) and the SUPER excitations [35, 51–53] were pursued in this work, even though both practical and theoretical challenges (discussed in Supporting Information Notes 4 and 5) led to unsuccessful preliminary investigations. The main obstacles encountered were related to low and high-frequency noise in the charge environment and to the high linear polarization of the emitter dipole, showing an absence of fine structure splitting. The outcomes from the acoustic phonon-assisted excitation measurements, combined with the knowledge acquired during the coherent excitation attempts, suggest that charge stabilization

is imperative for the advancement of the WSe₂ platform. This can be achieved by electrical control via the implementation of external gating. Having contacted devices will also provide control of the in-plane and out-of-plane electric fields, allowing spectral tuning of the emission by Stark shift. Additionally, understanding the exciton fine structure splitting in this type of quantum emitters will enable its active manipulation [54] and the development of tailored coherent excitation strategies.

VI. CONCLUSION

To summarize, we presented a systematic study on the single-photon emission properties of WSe₂ bilayer quantum emitters under various optical excitation schemes, such as above-band, near-resonant, and acoustic phonon-assisted. We demonstrated a fast recombination time of 1.33 ± 0.04 ns and a single-photon purity of 0.947 ± 0.079 under phonon-assisted excitation and compared these results to those under above-band and near-resonance excitations. It emerges that the decay dynamics get much simpler and immediate (about 1 order of magnitude faster). This effect is related to the fact that exciting near the resonance of the emitter via the efficient acoustic phonons avoids additional relaxation processes before populating the system. On the contrary, the extracted $g^{(2)}(0)$ values are similar within their error range for all three cases, suggesting that the single-photon purity of the studied bilayer quantum emitters is not heavily dependent on the excitation scheme. Additionally, the phonon-assisted excitation scheme generates a near resolution-limited ZPL emission of 0.072 nm and a 1.8-fold reduction in spectral diffusion compared to the above-band excitation. The importance of our result lay in the fact that transform-limited linewidth and spectral stability are essential requirements for the indistinguishability of the emitted single photons, which, however, was not measured here. Environmental effects are the major contributors to reduced single-photon indistinguishability in WSe₂ and, in general, in other layered materials. Achieving pure and indistinguishable emission from a confined state in WSe₂ requires charge environment stabilization and phonon decoupling. Our work contributes to the achievement of the above-mentioned goals by specifically focusing on the pumping scheme. As a further advancement, minimizing the interaction with the phonon bath can be achieved via off-resonant yet coherent excitation techniques, such as the SUPER scheme [51–53]. Understanding the impact of the pumping scheme on the characteristics of the single-photon emission represents a significant step towards the realization of deterministic high-quality single-photon sources in the WSe₂ platform.

VII. METHODS

Sample fabrication and preparation: The sample consists of a bilayer WSe₂ transferred on top of a 3-point star-shaped SiO₂ (HSQ) nanopillar on a Si/SiO₂ substrate. For the pillar fabrication, the sample was spin-coated with a negative electron-beam resist (Fox-06), and the star-shaped structures were patterned using a 100 kV electron beam lithography machine (JEOL 9500) with a dose of 11 000 $\mu\text{C}/\text{cm}^2$ and an electric current of 6 nA. The exposed resist was then developed in a (1:3) solution of AZ400K:H₂O. The HSQ resist is known to chemically change to SiO₂ after e-beam exposure, resulting in SiO₂ nanostructures of the same height as the resist (≈ 150 nm). The WSe₂ flake was exfoliated from bulk crystals using the conventional scotch-tape technique and subsequently transferred onto the patterned substrate by deterministic dry-transfer procedure. Finally, the defects were introduced in the flake lattice by electron-beam irradiation of the strained areas using the same 100 kV EBL machine with a dose of 1000 $\mu\text{C}/\text{cm}^2$ and a current of 6 nA.

Optical characterization: To perform photoluminescence measurements, we placed the WSe₂ mono and bilayer samples in a closed-cycle helium cryostat (at-toDRY 800, attocube systems AG) with a base temperature of 4 K. The cryostat is equipped with a microscope objective to focus the laser light onto the sample (NA = 0.8, 60 \times , attocube systems AG). The setup is configured in a cross-polarized configuration. For photoluminescence imaging, we employ a cooled sCMOS camera (Dhyana 400D, 4MP, Tucsen). To enable various excitation schemes, we employed a tunable OPO module (Chameleon Compact OPO-Vis, Coherent Inc.) pumped by a Ti:Sapphire laser (Chameleon Ultra II, Coherent Inc.) producing 150 fs pulses at 80 MHz repetition rate. To further optimize the laser spectral windows for various excitation methods, we also employed a home-built 4f pulse shaper ($f = 500$ mm) equipped with an 1800 groove/mm diffraction grating and a programmable single-mask transmissive spatial light modulator (SLM-S320, Jenoptik) in the Fourier plane. The SLM consists of 320 pixels, which helps to carve a narrow spectral range (FWHM ≈ 0.21 nm). To acquire the emission spectra, we utilized a fiber-coupled spectrometer (Horiba iHR 550) using either a 600 groove/mm or a 1200 groove/mm grating. For second-order correlation measurements, we employed a fiber-based Hanbury Brown and Twiss (HBT) interferometer coupled to superconducting nanowire single-photon detectors (SNSPD, ID218, ID Quantique) and time taggers (ID900, ID Quantique).

Data analysis: All the PL emissions from quantum emitters presented in the manuscript were fitted with a function that is a sum of a Lorentzian and a Gaussian. The Lorentzian contribution accounts for the homogeneous broadening of the line, while the Gaussian

distribution fits the phonon sideband. From the fitting, it is possible to extract the complete set of 6 parameters defining the distributions, together with the standard error for each one of them. The data obtained from time-resolved photoluminescence (TRPL) measurements was fitted with a sum of two uncorrelated exponentially decaying functions added to a constant background: $F_{\text{TRPL}}(\tau) = F_0 + A_1 e^{-(\tau - \tau_{01})/\tau_1} + A_2 e^{-(\tau - \tau_{02})/\tau_2}$, where F_0 accounts for the constant background, A_1 and A_2 are the amplitudes of the two exponential functions, τ_1 and τ_2 the two extracted decay constants, and τ_{01} and τ_{02} decay offset. The relative weight of the two of them is extracted as a percentage. In this way, we gain insight into the types of transitions that will contribute to the purity measurement. For the analysis of the second-order correlation measurements, the raw data is fitted with the following expression: $F_{\text{SOC}}(\tau) = B_1 [e^{-|\tau|/\tau_1} + e^{-|\tau|/\tau_2}] + B_2 \sum_n [e^{-|\tau + n\tau_{\text{rep}}|/\tau_1} + e^{-|\tau + n\tau_{\text{rep}}|/\tau_2}]$, where B_1 denotes the central peak area, B_2 the side peak areas, τ_1 and τ_2 the two extracted decay time constants, τ_{rep} the laser pulse repetition time, and n the index of each peak ($n = 0, \pm 1, \pm 2, \dots$). The $g^{(2)}(0)$ value is then calculated as $g^{(2)}(0) = F_{\text{SOC}}(0) / \max[F_{\text{SOC}}(\tau)]$.

Theory: The predicted population inversion under near-resonant excitation is obtained from theoretical modeling of a two-level emitter coupled to 2D acoustic phonons and a Gaussian laser pulse, and assuming that electron-phonon interaction is predominantly mediated by the coupling to 2D longitudinal acoustic phonons via the deformation potential mechanism. We consider a two-level system (ground state $|G\rangle$ and excited state $|X\rangle$) with Hamiltonian $H_0 = \hbar\omega_X^{(0)} |X\rangle\langle X|$ coupled to a bath of 2D acoustic phonons $H_{\text{ph}} = \sum_{\mathbf{k}} \hbar\omega_{\mathbf{k}} b_{\mathbf{k}}^\dagger b_{\mathbf{k}}$ via the interaction $H_{\text{int}} = \sum_{\mathbf{k}} \hbar g_{\mathbf{k}} b_{\mathbf{k}}^\dagger b_{\mathbf{k}} |X\rangle\langle X|$. The phonon influence is summarized by the phonon spectral density $J(\omega) = \alpha\omega^2 \exp(-\omega^2/\omega_c^2)$, which we extract by fitting the experimental data with the function

$$\Sigma(\omega) = A \text{Re} \left[\int_0^{+\infty} dt e^{\Phi(t)} e^{-i(\omega - \omega_X)t} e^{-Wt/2} \right]. \quad (1)$$

Here, $W = \Gamma + \gamma$ is the spectral width including the spontaneous emission rate Γ and an additional broadening γ beyond the transform-limited value, $\omega_X = \omega_X^{(0)} - D$ is the exciton frequency shifted by the polaron shift $D = \int_0^{+\infty} d\omega \omega^{-1} J(\omega)$, and the function $\Phi(t)$ is

$$\Phi(t) = \int_0^{+\infty} d\omega \frac{J(\omega)}{\omega^2} \left[\frac{\cos(\omega t) - 1}{\tanh(\hbar\omega/2k_{\text{B}}T)} - i \sin(\omega t) \right]. \quad (2)$$

Equation (1) is obtained from a polaron master equation [55], accounting for spontaneous emission and spectral broadening with two Lindblad terms $\Gamma \mathcal{L}_\sigma[\rho]$ and $\gamma \mathcal{L}_{\sigma^\dagger \sigma}[\rho]$, where $\mathcal{L}_A[\rho] = A\rho A^\dagger - \frac{1}{2}\{A^\dagger A, \rho\}$. From the phonon spectral density, we calculate the Huang-Rhys factor as $S = \int_0^{+\infty} d\omega \omega^{-2} J(\omega) = \frac{\sqrt{\pi}}{2} \omega_c \alpha$.

To model laser excitation, the system is also coupled to a pulsed laser at frequency ω_{laser} via $H_{\text{laser}} = \frac{\hbar}{2}\Omega(t)(e^{-i\omega_{\text{laser}}t}|X\rangle\langle G| + e^{i\omega_{\text{laser}}t}|G\rangle\langle X|)$, with a Gaussian pulse $\Omega(t) = \frac{\Theta}{\sqrt{\pi}t_p}e^{-(t/t_p)^2}$ and $\Theta = \int_{-\infty}^{+\infty} dt \Omega(t)$ the pulse area. The dynamics is obtained by solving the master equation for the reduced density operator $\rho(t)$ with the formalism of time-evolving matrix product operators (TEMPO) [56] as implemented in the OQUPY Python package [57], allowing to treat the phonon environment at a numerically-exact level. To calculate the $|X\rangle$ state population P_X after the laser pulse, the system is initialized in $|G\rangle$ at time $t = -3t_p$ and P_X is calculated as $P_X = \text{Tr}[|X\rangle\langle X|\rho(t)]|_{t=3t_p}$. The pulse detuning in frequency is defined with respect to the phonon-shifted exciton frequency as $\Delta\omega = \omega_{\text{laser}} - \omega_X$. The corresponding wavelength detuning is $\Delta\lambda = \lambda_{\text{laser}} - \lambda_X = 2\pi c(\omega_{\text{laser}}^{-1} - \omega_X^{-1})$.

ASSOCIATED CONTENT

Supporting Information

The Supporting Information is available free of charge at <https://.....>

NOTES

The authors declare no competing financial interest.

ACKNOWLEDGEMENT

The authors acknowledge support from the European Research Council (ERC-StG "TuneTMD", grant

no. 101076437), and the Villum Foundation (grant no. VIL53033). The authors also acknowledge the European Research Council (ERC-CoG "Unity", grant no. 865230), Carlsberg Foundation (grant no. CF21-0496), and support from the Independent Research Fund Denmark (Grant DFF-9041-00046B). N.G. acknowledges support from the European Union's Horizon 2020 Research and Innovation Program under the Marie Skłodowska-Curie Grant Agreement no. 861097. VR acknowledges financial support through the Austrian Science Fund FWF projects 10.55776/TAI556 (DarkEneT) and 10.55776/FG5. The authors acknowledge the clean-room facilities at DTU Nanolab – National Centre for Nano Fabrication and Characterization.

AUTHOR CONTRIBUTIONS

AP fabricated the final samples with support from CP and AM. CP performed all the optical measurements from the fabricated samples. CP and VR assembled a home-built pulse-shaping setup using the SLM. CP, PW, and AP contributed to experimental data analysis and processing. LV and JN performed theoretical calculations and fittings. BM conceived the idea, and LV, NG, and BM coordinated the project. CP took the lead in writing the manuscript. All authors discussed the results and contributed to the final manuscript.

VIII. REFERENCES

-
- [1] T. Heindel, J.-H. Kim, N. Gregersen, A. Rastelli, and S. Reitzenstein, Quantum dots for photonic quantum information technology, *Adv. Opt. Photon.* **15**, 613 (2023).
 - [2] P. G. Kwiat, K. Mattle, H. Weinfurter, A. Zeilinger, A. V. Sergienko, and Y. Shih, New high-intensity source of polarization-entangled photon pairs, *Phys. Rev. Lett.* **75**, 4337 (1995).
 - [3] H. S. Zhong, Y. Li, W. Li, L. C. Peng, Z. E. Su, Y. Hu, Y. M. He, X. Ding, W. Zhang, H. Li, L. Zhang, Z. Wang, L. You, X. L. Wang, X. Jiang, L. Li, Y. A. Chen, N. L. Liu, C. Y. Lu, and J. W. Pan, 12-Photon Entanglement and Scalable Scattershot Boson Sampling with Optimal Entangled-Photon Pairs from Parametric Down-Conversion, *Physical Review Letters* **121**, 250505 (2018).
 - [4] I. Aharonovich, D. Englund, and M. Toth, Solid-state single-photon emitters, *Nature Photonics* **2016** *10*:10, 631 (2016).
 - [5] H. Wang, Y.-M. He, T.-H. Chung, H. Hu, Y. Yu, S. Chen, X. Ding, M.-C. Chen, J. Qin, X. Yang, R.-Z. Liu, Z.-C. Duan, J.-P. Li, S. Gerhardt, K. Winkler, J. Jurkat, L.-J. Wang, N. Gregersen, Y.-H. Huo, Q. Dai, S. Yu, S. Höfling, C.-Y. Lu, and J.-W. Pan, Towards optimal single-photon sources from polarized microcavities, *Nature Photonics* **13**, 770 (2019).
 - [6] H. Ollivier, I. Maillette De Buy Wenniger, S. Thomas, S. C. Wein, A. Harouri, G. Coppola, P. Hilaire, C. Millet, A. Lemaitre, I. Sagnes, O. Krebs, L. Lanco, J. C. Loredó, C. Antón, N. Somaschi, and P. Senellart, Reproducibility of High-Performance Quantum Dot Single-Photon Sources, *ACS Photonics* **7**, 1050 (2020).
 - [7] N. Tomm, A. Javadi, N. O. Antoniadis, D. Najer, M. C. Löbl, A. R. Korsch, R. Schott, S. R. Valentin, A. D. Wieck, A. Ludwig, and R. J. Warburton, A bright and fast source of coherent single photons, *Nature Nanotechnology* **16**, 399 (2021).
 - [8] A. Srivastava, M. Sidler, A. V. Allain, D. S. Lembke, A. Kis, and A. Imamoglu, Optically active quantum dots in monolayer WSe₂, *Nature Nanotechnology* **10**, 491 (2015).
 - [9] P. Tonndorf, R. Schmidt, R. Schneider, J. Kern, M. Buscema, G. A. Steele, A. Castellanos-Gomez, H. S. J. van der Zant, S. Michaelis de Vasconcellos, and R. Brats-

- chitsch, Single-photon emission from localized excitons in an atomically thin semiconductor, *Optica* **2**, 347 (2015).
- [10] Y. M. He, G. Clark, J. R. Schaibley, Y. He, M. C. Chen, Y. J. Wei, X. Ding, Q. Zhang, W. Yao, X. Xu, C. Y. Lu, and J. W. Pan, Single quantum emitters in monolayer semiconductors, *Nature Nanotechnology* **10**, 497 (2015).
- [11] M. Koperski, K. Nogajewski, A. Arora, V. Cherkez, P. Mallet, J. Y. Veuillen, J. Marcus, P. Kossacki, and M. Potemski, Single photon emitters in exfoliated wse2 structures, *Nature nanotechnology* **10**, 503 (2015).
- [12] C. Chakraborty, L. Kinnischtzke, K. M. Goodfellow, R. Beams, and A. N. Vamivakas, Voltage-controlled quantum light from an atomically thin semiconductor, *Nature Nanotechnology* **10**, 507 (2015).
- [13] A. R-P Montblanch, M. Barbone, I. Aharonovich, M. Atatüre, and A. C. Ferrari, Layered materials as a platform for quantum technologies, *Nature Nanotechnology* **18**, 555 (2023).
- [14] Z. Gao, M. Q. Zhao, M. M. Alam Ashik, and A. T. Charlie Johnson, *Recent advances in the properties and synthesis of bilayer graphene and transition metal dichalcogenides* (2020).
- [15] K. Parto, S. I. Azzam, K. Banerjee, and G. Moody, Defect and strain engineering of monolayer WSe2 enables site-controlled single-photon emission up to 150 K, *Nature Communications* **12**, 10.1038/s41467-021-23709-5 (2021).
- [16] A. Micevic, N. Pettinger, A. Hötger, L. Sigl, M. Florian, T. Taniguchi, K. Watanabe, K. Müller, J. J. Finley, C. Kastl, and A. W. Holleitner, On-demand generation of optically active defects in monolayer WS2 by a focused helium ion beam, *Applied Physics Letters* **121**, 183101 (2022).
- [17] P. Tonndorf, O. Del Pozo-Zamudio, N. Gruhler, J. Kern, R. Schmidt, A. I. Dmitriev, A. P. Bakhtinov, A. I. Tartakovskii, W. Pernice, S. Michaelis De Vasconcellos, and R. Bratschitsch, On-Chip Waveguide Coupling of a Layered Semiconductor Single-Photon Source, *Nano Letters* **17**, 5446 (2017).
- [18] T. Cai, S. Dutta, S. Aghaeimeibodi, Z. Yang, S. Nah, J. T. Fourkas, and E. Waks, Coupling Emission from Single Localized Defects in Two-Dimensional Semiconductor to Surface Plasmon Polaritons, *Nano Letters* **17**, 6564 (2017).
- [19] M. Blauth, M. Jürgensen, G. Vest, O. Hartwig, M. Prechtel, J. Cerne, J. J. Finley, and M. Kaniber, Coupling Single Photons from Discrete Quantum Emitters in WSe2 to Lithographically Defined Plasmonic Slot Waveguides, *Nano Letters* **18**, 6812 (2018).
- [20] M. Brotons-Gisbert, J. P. Martínez-Pastor, G. C. Ballesteros, B. D. Gerardot, and J. F. Sánchez-Royo, Engineering light emission of two-dimensional materials in both the weak and strong coupling regimes, *Nanophotonics* **7**, 253 (2018).
- [21] K. Barthelmi, J. Klein, A. Hötger, L. Sigl, F. Sigger, E. Mitterreiter, S. Rey, S. Gyger, M. Lorke, M. Florian, F. Jahnke, T. Taniguchi, K. Watanabe, V. Zwiller, K. D. Jöns, U. Wurstbauer, C. Kastl, A. Weber-Bargioni, J. J. Finley, K. Müller, and A. W. Holleitner, Atomistic defects as single-photon emitters in atomically thin MoS2, *Applied Physics Letters* **117**, 070501 (2020).
- [22] H. Zhao, M. T. Pettes, Y. Zheng, and H. Htoon, Site-controlled telecom-wavelength single-photon emitters in atomically-thin MoTe2, *Nature Communications* **2021**:1 **12**, 1 (2021).
- [23] J.-P. So, H.-R. Kim, H. Baek, K.-Y. Jeong, H.-C. Lee, W. Huh, Y. S. Kim, K. Watanabe, T. Taniguchi, J. Kim, C.-H. Lee, and H.-G. Park, Electrically driven strain-induced deterministic single-photon emitters in a van der waals heterostructure, *Science Advances* **7**, 10.1126/sciadv.abj3176 (2021).
- [24] T. Gao, M. von Helversen, C. Antón-Solanas, C. Schneider, and T. Heindel, Atomically-thin single-photon sources for quantum communication, *npj 2D Materials and Applications* **7**, 10.1038/s41699-023-00366-4 (2023).
- [25] O. Iff, D. Tedeschi, J. Martín-Sánchez, M. Moczaladusowska, S. Tongay, K. Yumigeta, J. Taboada-Gutiérrez, M. Savaresi, A. Rastelli, P. Alonso-González, S. Höfling, R. Trotta, and C. Schneider, Strain-Tunable Single Photon Sources in WSe2 Monolayers, *Nano Letters* **19**, 6931 (2019).
- [26] L. Linhart, M. Paur, V. Smejkal, J. Burgdörfer, T. Mueller, and F. Libisch, Localized Intervalley Defect Excitons as Single-Photon Emitters in WSe2, *Physical Review Letters* **123**, 10.1103/PhysRevLett.123.146401 (2019).
- [27] J. C. Drawer, V. N. Mitryakhin, H. Shan, S. Stephan, M. Gittinger, L. Lackner, B. Han, G. Leibelng, F. Eilenberger, R. Banerjee, S. Tongay, K. Watanabe, T. Taniguchi, C. Lienau, M. Silies, C. Anton-Solanas, M. Esmann, and C. Schneider, Monolayer-Based Single-Photon Source in a Liquid-Helium-Free Open Cavity Featuring 65% Brightness and Quantum Coherence, *Nano Letters* **23**, 8683 (2023).
- [28] V. N. Mitryakhin, A. Steinhoff, J.-C. Drawer, H. Shan, M. Florian, L. Lackner, B. Han, F. Eilenberger, S. A. Tongay, K. Watanabe, T. Taniguchi, C. Antón-Solanas, A. Predojević, C. Gies, M. Esmann, and C. Schneider, Engineering the Impact of Phonon Dephasing on the Coherence of a WSe 2 Single-Photon Source via Cavity Quantum Electrodynamics , *Physical Review Letters* **132**, 206903 (2024).
- [29] R. S. Daveau, T. Vandekerckhove, A. Mukherjee, Z. Wang, J. Shan, K. F. Mak, A. N. Vamivakas, and G. D. Fuchs, Spectral and spatial isolation of single tungsten diselenide quantum emitters using hexagonal boron nitride wrinkles, *APL Photonics* **5**, 096105 (2020).
- [30] H. Akbari, S. Biswas, P. K. Jha, J. Wong, B. Vest, and H. A. Atwater, Lifetime-Limited and Tunable Quantum Light Emission in h-BN via Electric Field Modulation, *Nano Letters* **22**, 7798 (2022).
- [31] M. Reindl, J. H. Weber, D. Huber, C. Schimpf, S. F. Covre Da Silva, S. L. Portalupi, R. Trotta, P. Michler, and A. Rastelli, Highly indistinguishable single photons from incoherently excited quantum dots, *Physical Review B* **100**, 155420 (2019).
- [32] E. B. Flagg, A. Muller, S. V. Polyakov, A. Ling, A. Migdall, and G. S. Solomon, Interference of Single Photons from Two Separate Semiconductor Quantum Dots, *Phys. Rev. Lett.* **104**, 10.1103/PhysRevLett.104.137401 (2010).
- [33] Y. M. He, Y. He, Y. J. Wei, D. Wu, M. Atatüre, C. Schneider, S. Höfling, M. Kamp, C. Y. Lu, and J. W. Pan, On-demand semiconductor single-photon source with near-unity indistinguishability, *Nature Nanotechnology* **2013** **8**:3 **8**, 213 (2013).
- [34] S. E. Thomas, M. Billard, N. Coste, S. C. Wein, Priya, H. Ollivier, O. Krebs, L. Tazaïrt, A. Harouri,

- A. Lemaitre, I. Sagnes, C. Anton, L. Lanco, N. Somaschi, J. C. Loredó, and P. Senellart, Bright Polarized Single-Photon Source Based on a Linear Dipole, *Physical Review Letters* **126**, 10.1103/PhysRevLett.126.233601 (2020).
- [35] L. Vannucci, J. F. Neto, C. Piccinini, A. Paralikis, N. Gregersen, and B. Munkhbat, Single-photon emitters in wse2: The critical role of phonons on excitation schemes and indistinguishability (2024), [arXiv:2402.10897](https://arxiv.org/abs/2402.10897).
- [36] A. Paralikis, C. Piccinini, A. A. Madigawa, P. Metuh, L. Vannucci, N. Gregersen, and B. Munkhbat, [Tailoring Polarization in WSe2 Quantum Emitters through Deterministic Strain Engineering](#) (2024).
- [37] C. Schneider, K. Winkler, M. D. Fraser, M. Kamp, Y. Yamamoto, E. A. Ostrovskaya, and S. Höfling, [Exciton-polariton trapping and potential landscape engineering](#) (2017).
- [38] S. Reitzenstein, T. Heindel, C. Kistner, F. Albert, T. Braun, C. Hopfmann, P. Mrowinski, M. Lerner, C. Schneider, S. Höfling, M. Kamp, and A. Forchel, Electrically driven quantum dot micropillar light sources, *IEEE Journal on Selected Topics in Quantum Electronics* **17**, 1670 (2011).
- [39] G. Bacher, R. Weigand, J. Seufert, V. D. Kulakovskii, N. A. Gippius, A. Forchel, K. Leonardi, D. Hommel, K. Leonardi, and D. Hommel, Biexciton versus Exciton Lifetime in a Single Semiconductor Quantum Dot, *Physical Review Letters* **83**, 4417 (1999).
- [40] C. K. Dass, M. A. Khan, G. Clark, J. A. Simon, R. Gibson, S. Mou, X. Xu, M. N. Leuenberger, and J. R. Hendrickson, Ultra-Long Lifetimes of Single Quantum Emitters in Monolayer WSe2/hBN Heterostructures, *Advanced Quantum Technologies* **2**, 1900022 (2019).
- [41] M. Amani, P. Taheri, R. Addou, G. H. Ahn, D. Kiriya, D. H. Lien, J. W. Ager, R. M. Wallace, and A. Javey, Recombination Kinetics and Effects of Superacid Treatment in Sulfur- and Selenium-Based Transition Metal Dichalcogenides, *Nano Letters* **16**, 2786 (2016).
- [42] Y. Ye, X. Dou, K. Ding, Y. Chen, D. Jiang, F. Yang, and B. Sun, Single photon emission from deep-level defects in monolayer WSe2, *Physical Review B* **95**, 10.1103/PhysRevB.95.245313 (2017).
- [43] H. Terrones and M. Terrones, Bilayers of transition metal dichalcogenides: Different stackings and heterostructures, *Journal of Materials Research* **29**, 373 (2014).
- [44] M. von Helversen, L. Greten, I. Limame, C.-W. Shih, P. Schlaugat, C. Anton-Solanas, C. Schneider, B. Rosa, A. Knorr, and S. Reitzenstein, Temperature dependent temporal coherence of metallic-nanoparticle-induced single-photon emitters in a WSe2 monolayer, *2D Materials* 10.1088/2053-1583/acfb20 (2023).
- [45] J. Lindlau, M. Selig, A. Neumann, L. Colombier, J. Förste, V. Funk, M. Förg, J. Kim, G. Berghäuser, T. Taniguchi, K. Watanabe, F. Wang, E. Malic, and A. Högele, The role of momentum-dark excitons in the elementary optical response of bilayer WSe2, *Nature Communications* **9**, 10.1038/s41467-018-04877-3 (2018).
- [46] S. Kumar, M. Brotons-Gisbert, R. Al-Khuzheyri, A. Branny, G. Ballesteros-Garcia, J. F. Sánchez-Royo, and B. D. Gerardot, Resonant laser spectroscopy of localized excitons in monolayer WSe2, *Optica* **3**, 882 (2016).
- [47] N. Mounet, M. Gibertini, P. Schwaller, D. Campi, A. Merkys, A. Marrazzo, T. Sohier, I. E. Castelli, A. Cepellotti, G. Pizzi, and N. Marzari, Two-dimensional materials from high-throughput computational exfoliation of experimentally known compounds, *Nature Nanotechnology* **13**, 246 (2018).
- [48] N. Mounet, M. Gibertini, P. Schwaller, D. Campi, A. Merkys, A. Marrazzo, T. Sohier, I. E. Castelli, A. Cepellotti, G. Pizzi, and N. Marzari, [Two-dimensional materials from high-throughput computational exfoliation of experimentally known compounds](#) (2018).
- [49] S. Hastrup, M. Strange, M. Pandey, T. Deilmann, P. S. Schmidt, N. F. Hinsche, M. N. Gjerding, D. Torelli, P. M. Larsen, A. C. Riis-Jensen, J. Gath, K. W. Jacobsen, J. J. Mortensen, T. Olsen, and K. S. Thygesen, The Computational 2D Materials Database: high-throughput modeling and discovery of atomically thin crystals, *2D Materials* **5**, 042002 (2018).
- [50] M. N. Gjerding, A. Taghizadeh, A. Rasmussen, S. Ali, F. Bertoldo, T. Deilmann, N. R. Knøsgaard, M. Kruse, A. H. Larsen, S. Manti, T. G. Pedersen, U. Petralanda, T. Skovhus, M. K. Svendsen, J. J. Mortensen, T. Olsen, and K. S. Thygesen, Recent progress of the Computational 2D Materials Database (C2DB), *2D Materials* **8**, 044002 (2021).
- [51] T. K. Bracht, M. Cosacchi, T. Seidelmann, M. Cygorek, A. Vagov, V. M. Axt, T. Heindel, and D. E. Reiter, Swing-up of quantum emitter population using detuned pulses, *PRX Quantum* **2**, 040354 (2021).
- [52] Y. Karli, F. Kappe, V. Remesh, T. K. Bracht, J. Münzberg, S. Covre Da Silva, T. Seidelmann, V. M. Axt, A. Rastelli, D. E. Reiter, and G. Weihs, SUPER Scheme in Action: Experimental Demonstration of Red-Detuned Excitation of a Quantum Emitter, *Nano Letters* **22**, 6567 (2022).
- [53] K. Boos, F. Sbresny, S. K. Kim, M. Kremser, H. Riedl, F. W. Bopp, W. Rauhaus, B. Scaparra, K. D. Jöns, J. J. Finley, K. Müller, and L. Hanschke, Coherent swing-up excitation for semiconductor quantum dots, *Advanced Quantum Technologies* **7**, 2300359 (2024).
- [54] M. M. Glazov, F. Dirnberger, V. M. Menon, T. Taniguchi, K. Watanabe, D. Bougeard, J. D. Ziegler, and A. Chernikov, Exciton fine structure splitting and linearly polarized emission in strained transition-metal dichalcogenide monolayers, *Phys. Rev. B* **106**, 125303 (2022).
- [55] L. Vannucci and N. Gregersen, Highly efficient and indistinguishable single-photon sources via phonon-decoupled two-color excitation, *Physical Review B* **107** (2023).
- [56] A. Strathearn, P. Kirton, D. Kilda, J. Keeling, and B. W. Lovett, Efficient non-Markovian quantum dynamics using time-evolving matrix product operators, *Nature Communications* 2018 9:1 **9**, 1 (2018).
- [57] The TEMPO collaboration, [OQuPy: A Python 3 package to efficiently compute non-Markovian open quantum systems](#) (2020).